Advances in Concrete Construction, *Vol. 8, No. 3 (2019) 173-185*
DOI: https://doi.org/10.12989/acc.2019.8.3.173

Investigations of different steel layouts on the seismic behavior of transition steel-concrete composite connections

Liangjie Qi[1,2a], Jianyang Xue*[1] and Lei Zhai[1]

[1]*Department of Civil Engineering, Xi'an University of Architecture and Technology, Xi'an 710055, China*
[2]*Disaster Prevention Research Institute, Kyoto University, Uji 611011, Japan*

(*Received September 11, 2018, Revised May 17, 2019, Accepted June 4, 2019*)

Abstract. This article presents a comparative study of the effect of steel layouts on the seismic behavior of transition steel-concrete composite connections, both experimental and analytical investigations of concrete filled steel tube-reinforced concrete (CFST-RC) and steel reinforecd concrete-reinforced concrete (SRC-RC) structures were conducted. The steel-concrete composite connections were subjected to combined constant axial load and lateral cyclic displacements. Tests were carried out on four full-scale connections extracted from a real project engineering with different levels of axial force. The effect of steel layouts on the mechanical behavior of the transition connections was evaluated by failure modes, hysteretic behavior, backbone curves, displacement ductility, energy dissipation capacity and stiffness degradation. Test results showed that different steel layouts led to significantly different failure modes. For CFST-RC transition specimens, the circular cracks of the concrete at the RC column base was followed by steel yielding at the bottom of the CFST column. While uncoordinated deformation could be observed between SRC and RC columns in SRC-RC transition specimens, the crushing and peeling damage of unconfined concrete at the SRC column base was more serious. The existences of I-shape steel and steel tube avoided the pinching phenomenon on the hysteresis curve, which was different from the hysteresis curve of the general reinforced concrete column. The hysteresis loops were spindle-shaped, indicating excellent seismic performance for these transition composite connections. The average values of equivalent viscous damping coefficients of the four specimens are 0.123, 0.186 and 0.304 corresponding to the yielding point, peak point and ultimate point, respectively. Those values demonstrate that the transition steel-concrete composite connections have great energy dissipating capacity. Based on the experimental research, a high-fidelity ABAQUS model was established to further study the influence of concrete strength, steel grade and longitudinal reinforcement ratio on the mechanical behavior of transition composite connections.

Keywords: steel layout; transition composite connections; concrete filled steel tube; steel reinforced concrete; axial compression ratio

1. Introduction

RC columns have been widely used in common buildings and bridge piers in the past; nowadays steel can be deployed together with reinforced concrete to further increase the axial and seismic behavior (Han and An 2014). The steel-concrete composite combination is divided into several categories including concrete filled steel tube (CFST) and steel reinforced concrete (SRC) which are extensively used for the real project engineering in the high seismic zone recently because of their excellent ductility and energy absorption capacity (Xue *et al.* 2016, Xu *et al.* 2019). The cross-sectional area often increases visibly at lower floor because of the occurrence of shear failure at the bottom weak story (shown in Fig. 1), yet the increasing area accounts for substantial amount of residential space and looks unaesthetic to some extent; on the other hand, the composite cross-section with steel can increase the total strength and reduce the sectional dimensions. Besides that, a sudden change of stiffness is rather noticeable if the full-length column adopts the same material but different sectional areas, the employed steel, either in CFST or SRC, can minimize the stiffness variation (Qi *et al.* 2017).

The rectangular-circular transition columns often appear in irregular key structures, especially in Chinese Traditional-style buildings (Xue and Qi 2016, Qi and Xue 2018, Qi *et al.* 2018), just as shown in Fig. 2. The red part represents the investigated specimens and the black dot circle shows the transition region of upper composite part and lower RC part. The transition region is used to install unique components called "Center block", "Purlin arch" and "Bracket". Besides this kind of key architecture in China, there are also some other important architectures adopting this kind of column for the sake of aesthetics and uniqueness.

Plenty of scholars conducted numerical studies on the seismic performance of RC columns, normally, a pronounced pinching phenomenon can be observed on the hysteresis curves (Kunnath *et al.* 1997, D'Ambrisi and Filippou 1999, Lowes and Altoontash 2003, Tirasit and Kawashima 2007, Verderame *et al.* 2008). To avoid the poor energy absorption capacity of RC components,

*Corresponding author, Professor
E-mail: jianyang_xue@163.com
[a]Ph.D.
E-mail: qiliangjie@gmail.com

http://www.techno-press.org/?journal=acc&subpage=7
ISSN: 2287-5301 (Print), 2287-531X (Online)

(a) Overall view

(b) Close-up view

Fig. 1 Shear failure on ground floor

numerous studies in the hybrid structural components have been performed in recent years. Wang (Wang *et al.* 2015) tested eight concrete-encased CFST box specimens and eight RC box counterparts under constant axial load and cyclic lateral load at the midspan, the test results showed that the performances of CFST box columns, including the lateral resistance, stiffness degradation, ductility, and energy dissipation capacity, were significantly improved compared with the corresponding RC box columns. Yadav *et al.* studied the CFST-RC columns connected with RC-web under cyclic loading test; it proved that the CFST-RC columns behaved in a ductile manner, the ductility of columns increased with the increase in the diameter of steel tube and decreased with the increase of the RC-web thickness (Yadav *et al.* 2018). Besides the experimental investigations, a nonlinear finite element model was developed to study the behavior of square CFST column and RC column with the same material and cross-section sizes using ANSYS by Fu *et al.* (Fu *et al.* 2011), the results of FEA indicated that the bearing capacity and deformation capacity of CFST columns was greater than that of RC column.

Apart from using CFST columns, SRC-RC transition column is another alternation to enhance the mechanical behavior of the traditional RC column. Wu *et al.* (Wu *et al.* 2008, Wu *et al.* 2010, Wu *et al.* 2013, Wu *et al.* 2016) performed a systematical and comprehensive study on the failure mechanism, strength and stiffness degradation, shear capacity, stress transmission and bonding effect of SRC-RC hybrid structures. Sixteen SRC-RC transition columns and one RC column subjected to cyclic shear loading were carried out. The results showed that the ductility factor increased from 1.97 for RC columns to 5.99 for SRC-RC counterparts, and the seismic behavior was found to be the most optimal in this study when the embedment length of the shaped steel is 3/5 of the height of the entire RC column.

All of the above-mentioned literature focused on the columns without the variations of cross-sectional area, and thus the issue of stiffness abrupt change due to different geometrical specifications remains. To overcome this defect, the transition steel-concrete composite connections was put forward, the CFST or SRC columns was deployed in the upper column, as shown in Fig. 3, to take advantage of the high strength and ductility of steel material. The main objective of this experimental study is to provide insight into the structural behavior of the innovative transition connections to bridge the gap between the actual engineering and the research projects.

In this study, a comparative study is presented to illustrate the effect of steel layouts on the seismic behavior of transition steel-concrete composite connections, the influence of various axial compression ratio was considered. This configuration connects the top CFST or SRC and the bottom RC circular columns. The quasi-static test was conducted to investigate the failure modes, the load-displacement hysteresis hoops, backbone curves, ductility and energy dissipation capacity. Additionally, a high-fidelity FEA model analyses were established to compare with the experimental results, then a further detailed parametric study was performed to study the influence of concrete strength, steel grade and longitudinal

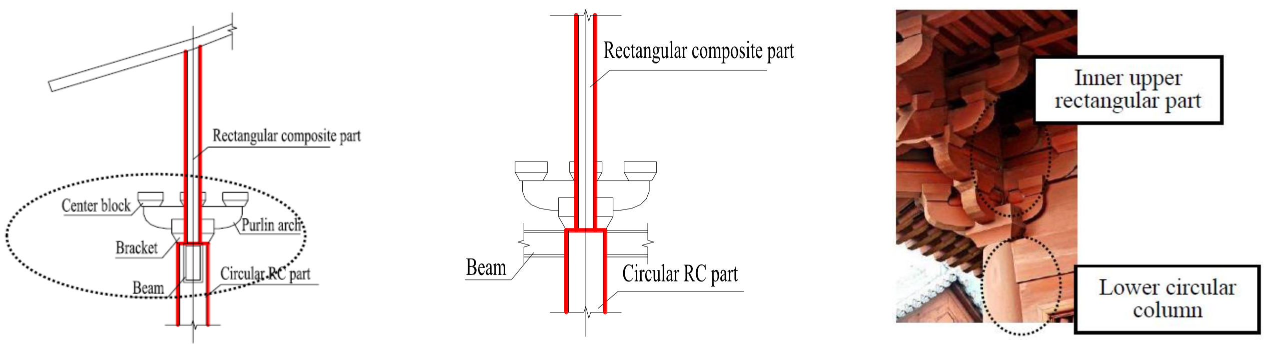

(a) Side view (b) Front view (c) Practical engineering

Fig. 2 Prototype of the specimens

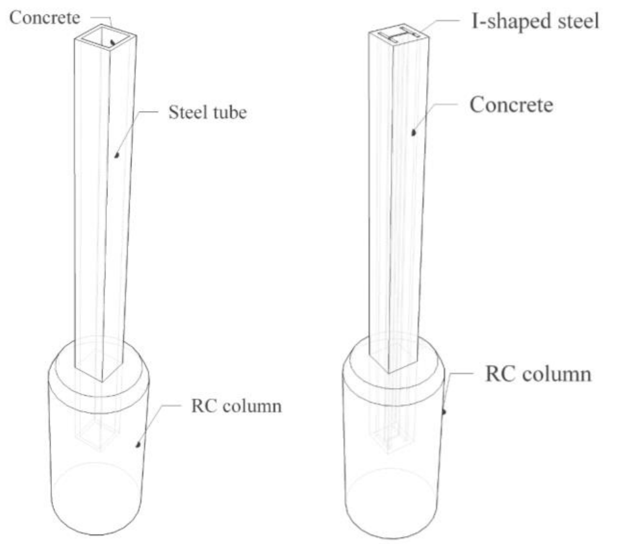

(a) CFST-RC (b) SRC-RC

Fig. 3 Transition steel-concrete composite connections

reinforcement ratio on the mechanical behavior of transition composite connections.

2. Experimental program

2.1 Test specimen

The full-scale test specimens were extracted from the real project engineering to avoid the scaling error. To study the influence of steel forms on seismic performance of transition steel-concrete composite connections, CFST-RC and SRC-RC structures were investigated in this project. For CFST-RC connections, the upper square columns deployed 180×180×8 mm steel tube filled with C30 (Cubic compressive standard strength of 30 MPa) concrete filled in the tube core. The SRC-RC connections employed the No.10 I-shape steel instead of steel tube, the total height, flange width, web thickness and flange thickness of I-shape steel section are 100 mm, 68 mm, 4.5 and 7.6 mm, respectively. The transition sections between the upper and lower columns are the stress concentration region under cyclic loading, so the lower RC circular columns are slightly shorter than that of the prototype and the steel inserted into the circular RC column to a depth varied from 1080 mm to 1400 mm in this project. The details and general dimensions of the specimens are illustrated in Fig. 4. According to the standard of steel-concrete composite structures (JGJ 138-2001), #19 steel stubs with the spacing of 150 mm were adopted during the fabrication of the specimen to enhance the bonding between steel and concrete (see Fig. 4).

Based on the previous studies, the axial compression ratio (ACR) has a significant influence on the ductility and strength of structures (Chen *et al.* 2015). In this study, two different ACRs were adopted, ACR of 0.3 was assigned to the specimen CFST-1 and SRC-1 while 0.6 was applied to the remaining two samples. The four specimens had the same slenderness (*KL/r*) of 61.35. All of the steel plates, including the I-shape steel and steel tube, were made of Q235 steel (nominal f_y=235 MPa). The longitudinal reinforcement in the lower column consisted of six #20 steel bars (ρ=1.13%) made from HRB 400 (f_y=400 MPa) steel, and the upper square column deployed four #20 longitudinal bars made of HRB 400 steel. Circular column stirrups, made from HPB 235 (f_y=235 MPa) steel, consisted of #10 steel bars (ρ=4.23%) at a spacing of 100 mm for CFST-RC specimens and #8 steel bars at a spacing of 100mm for SRC-RC specimens. The concrete protective cover was 25 mm. All the tested steel coupons were taken

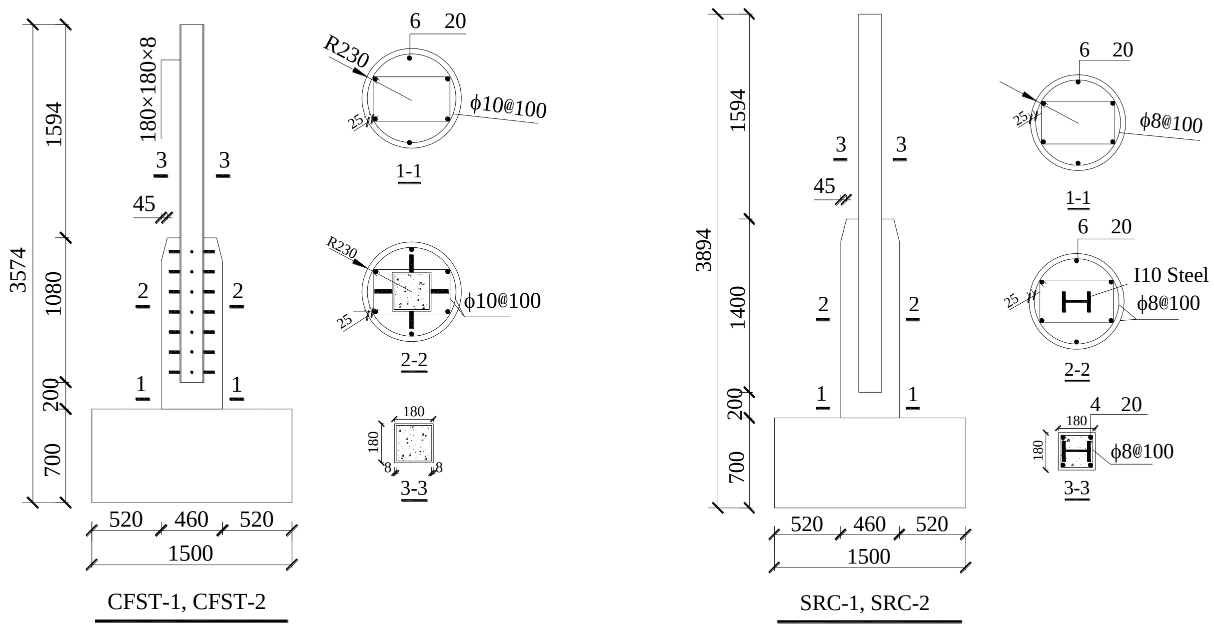

(a) CFST (b) SRC

Fig. 4 Dimensions and details of specimens (Unit: mm)

Table 1 Material mechanical properties

Category	Material	f_y (MPa)	f_u (MPa)	E_s (MPa)	Elongation /%	f_{cu} (MPa)
CFST-RC	Steel tube	323.8	450.2	1.91×10^5	30.4	/
	# 10 steel bar	317.2	517.5	2.32×10^5	26.3	/
	# 20 steel bar	431.6	625.0	2.01×10^5	25.0	/
	Concrete-CFST	/	/	/	/	35.46
	Concrete-RC	/	/	/	/	40.57
SRC-RC	I-10 shape steel	317.3	453.4	1.97×10^5	28.4	/
	# 8 steel bar	372.4	520.0	1.99×10^5	30.1	/
	# 20 steel bar	385.2	533.2	2.03×10^5	27.5	/
	Concrete-SRC	/	/	/	/	35.02
	Concrete-RC	/	/	/	/	41.30

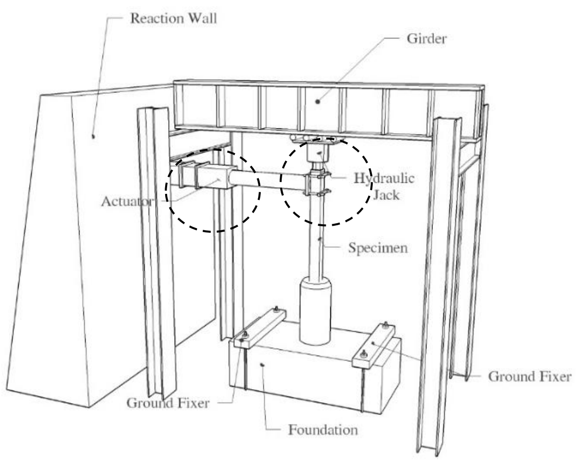

(a) General view

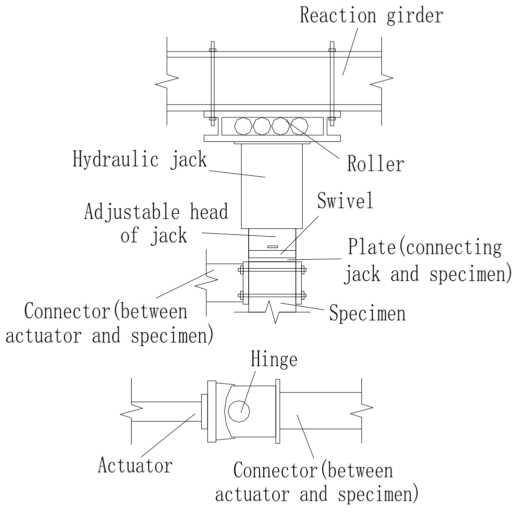

(b) Detailed construction

Fig. 5 Test setup

according to "Steel and steel products-location and preparation of test pieces for mechanical testing (GB/T 2975-1998)". To overcome the one-time concrete pouring imperfection and curing error, the pouring was divided into two stages corresponding to different concrete locations. The measured material mechanical properties are shown in Table 1.

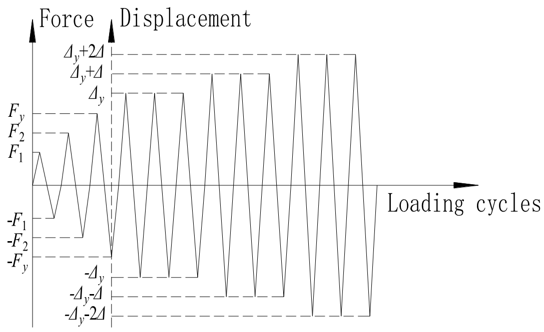

Fig. 6 Loading history

2.2 Test setup and protocol

The test setup is shown in Fig. 5, the quasi-static test can be divided into two stages. The axial force was applied at first by the vertical hydraulic jack; rollers were used to reduce the friction between the girder and the jack and a swivel was adopted to ensure the load vertically. The vertical load remained constant during the entire loading process.

Secondly, the horizontal loading displacement was applied on the top of specimens by a 500kN MTS973 actuator, and two hinges were used to guarantee the load horizontal (Fig. 5(b)). The force-displacement hybrid control protocol was deployed in these experiments. The moment switching from force mechanism to displacement was determined by the yield point which was represented by the inflection points on the hysteresis curves, each force-loaded level cycled once before yielding, then the loading cycled three times in the subsequent displacement-controlling stage. The diagrammatic loading protocol is illustrated in Fig. 6. The test ended when the load reduced to 85% of the peak load.

2.3 Distributions of strain gauges and LVDTs

The measurement layout of strain gauges and Linear Variable Differential Transducers (LVDTs) of CFST-1 is shown in Fig. 7, the measuring points of the other three specimens are identical as CFST-1. The applied force on the column top were measured by the loading actuator. Strain gauges were attached at different key stress locations on steel plates (steel tube and I-shape steel) and steel bars. Test data were acquired by the Tokyo TDS-602 system.

3. Results and discussion

3.1 Failure modes

For CFST series, multiple circumferential cracks appeared in the lower RC column at the initial loading phase. The cracking concrete at the top surface of the RC column extended obliquely from the corner of the steel tube to the outside region, then more vertical cracks were observed in this part. Due to the restraining effect of the upper rectangular CFST steel pipe, there was no obvious macroscopic failure phenomenon in the upper CFST

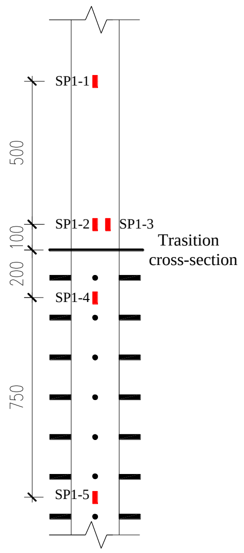

(a) Steel plate

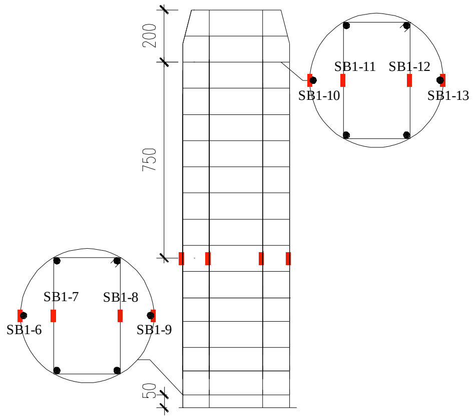

(b) Steel bars

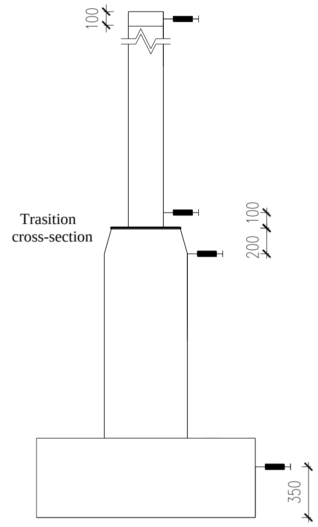

(c) Displacement transducers

Fig. 7 Arrangement of measuring points (CFST-1)

(a) CFST-1 (b) CFST-2 (c) SRC-1 (d) SRC-2

Fig. 8 Failure modes

column. With the increase of the load, the steel tube and the steel bars at RC column base yielded successively, and the circular cracks were observed at the same height with different stirrups. As the controlled displacement gradually increased, the vertical crack in the RC column extended to form a loop-closed diagonal crack. After that a small amount of concrete at the RC column base was crushed and peeled off, consequently, exposing the embedded reinforcing bars. Due to the larger vertical load, CFST-2 experienced a greater bending moment and had a larger concrete peeling range when compared with CFST-1. The ultimate failure mode of the CFST-RC transition connection under repeated loading was primarily due to bending failure, and the plastic hinges with certain rotation ability can be formed at the bottom of both CFST and RC columns.

For SRC-RC transition columns, because the bending stiffness of the lower RC circular column was much larger than that of the upper SRC column, the main deformation was aggregated in the upper SRC column. The most vulnerable region was the transition part between upper and lower columns, a large number of horizontally distributed cracks appeared in this region. The first yielding of the SRC column base was followed by gradual yielding of longitudinal reinforcement of the SRC column, but only a small amount of longitudinal reinforcement of the RC column base yielding occurred. For SRC-2 specimen, the failure was similar to SRC-1, but the crack developed more rapid than SRC-1, and the degree of concrete crushing and peeling was more severe. The specimens were all subjected to bending failure, and at the end of the loading, an obvious plastic hinge was formed in the transition areas. The failure modes are shown in Fig. 8, for CFST-RC specimens, only

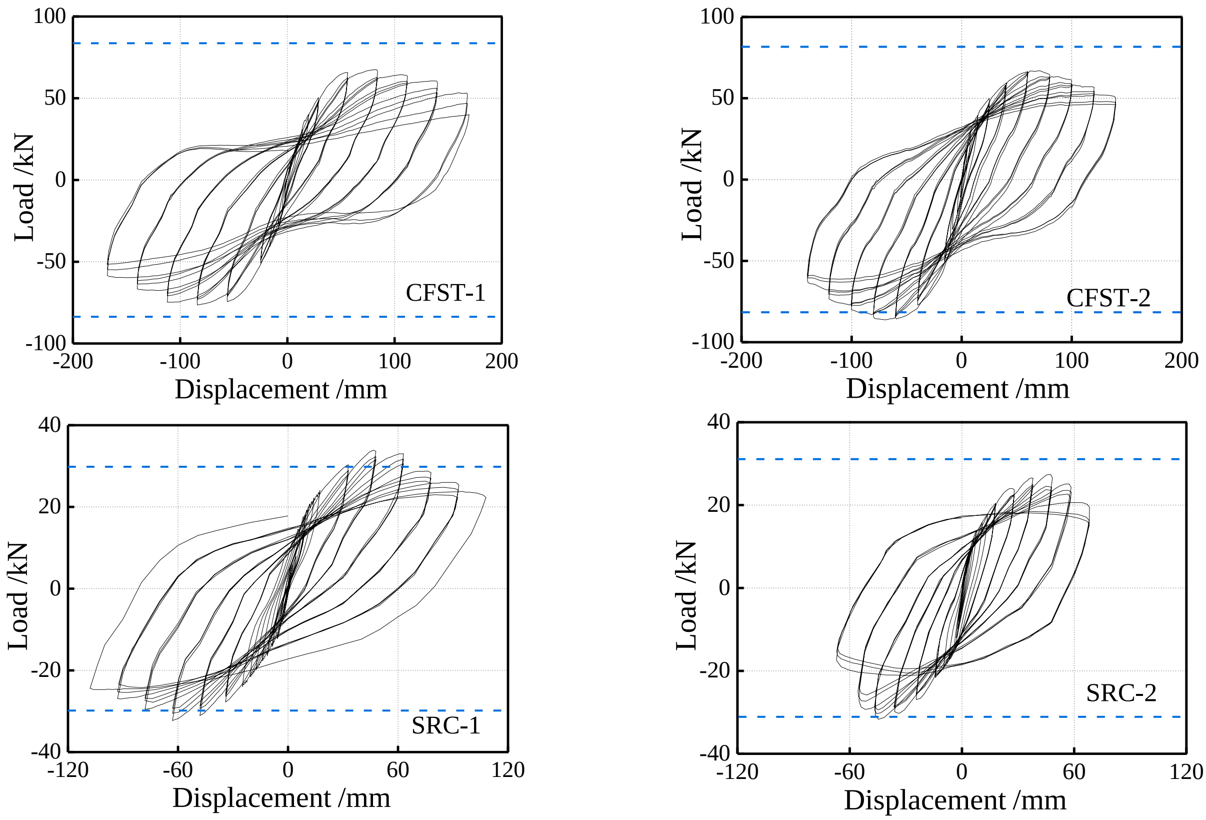

Fig. 9 Hysteretic loops

the lower circular RC columns are shown because no macroscopic failure was observed in the upper CFST square columns.

It can be seen that different steel layout resulted in significantly different failure modes. Though the cross-sectional inertia moment of the lower circular column is larger than the upper rectangular one, the apparent damage was shown at the bottom end of the RC column for CFST-RC specimens, the reason is that the steel tube of upper CFST column provided enough restraining effect on the inner concrete. The steel tube ruined the unconfined concrete at the transition section, and more vertical cracks were developed from the root of the tube angle. However, the I-shape steel only provided constraint to the confined concrete for SRC-RC specimens; the cracks and spalling of unconfined concrete could be clearly observed during the test. In addition, the cross-sectional steel ratio (15.99% of CFST specimens while 4.41% of SRC specimens) also resulted in these results.

3.2 Hysteretic behavior

The hysteresis curves exhibit the seismic performance and essential mechanical characteristics, including the initial stiffness, bearing strength and so on. Fig. 9 shows the hysteresis behavior of the four specimens, which reveals the relations between the lateral loads and displacements at the top of the upper square columns.

The blue dashed line in Fig. 9 is the maximum strength capacity derived based on the theoretical method in Chinese Composite Structures Design Code (JGJ 138-2016) and Chinese Concrete Design Code (GB 50010-2010), the calculation results indicate that the transition section between rectangular and circular columns reached the cross-sectional maximum strength first, which corresponds to the aforementioned experimental phenomena.

The following conclusions can be drawn.

(1) At the initial stage of loading, the specimens are in the elastic stage and the load and displacement are linear, the area surrounded by the hysteresis loop is relatively small, and thus the residual deformation and energy dissipation can be neglected.

(2) As the loading displacements increase, the hysteresis curves become spindle-shaped, the energy dissipation capacity is fully exerted and the stiffness degradation is significant. In the cyclic loading at the same loading displacement level, circular cracking damage of the concrete in the RC column of the CFST-RC specimen is more pronounced with the increase of loading cycles, while for SRC-RC series specimens, the cracks appeared densely on the upper SRC column base; either of the two damage patterns has adverse impact on the maximum load capacity.

(3) The influence of the axial compression ratio (ACR) is obvious; the coordinated deformation capacity of the smaller ACR specimen is slightly better. When ACR increases, the area surrounded by the hysteresis curve is larger, indicating higher energy dissipation; however, the displacement ductility is decreased and the stiffness degradation rate is faster.

(4) With the existence of I-shape steel and steel tube, the pinching phenomenon on hysteresis curve can be avoided, which is normally observed on RC column. The shape of

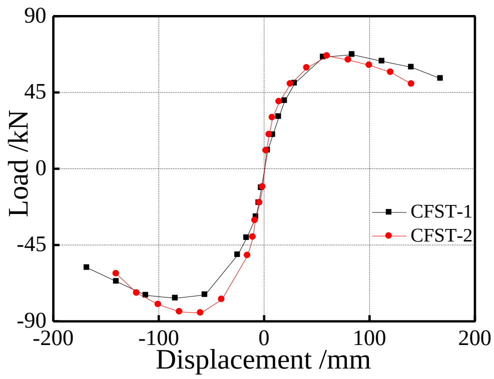

(a) CFST series

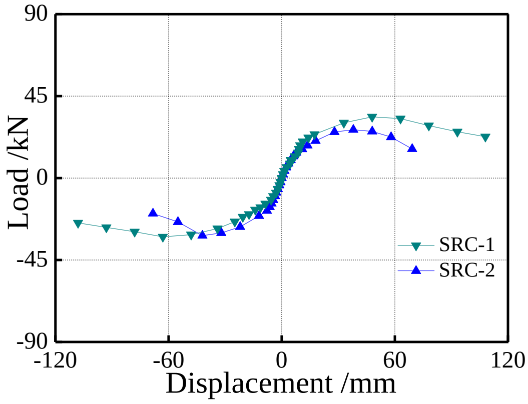

(b) SRC series

Fig. 10 Backbone curves of specimens

hysteresis curve is similar to that of the steel structure regardless of the layout form of steel, indicating superior seismic performance and greater toughness than RC structures.

(5) The strength capacity is governed by the steel ratio inside the section, for instance, the strength capacity of CFST-1 can reach twice as much as that of the SRC-1, which is attributed to its higher steel ratio.

3.3 Backbone curve

The backbone curve is the most important basis of the elastoplastic analyses, which reflects the mutual relationship between the lateral load and the corresponding displacement. The measured backbone curves of the four specimens are shown in Fig. 10. The lateral load and displacement are obtained by the horizontal actuator and top displacement transducer, respectively, the yield point is determined by the Universal Yield Moment Method (Xue and Qi 2016). The characteristic points are listed in Table 2.

(1) All of the backbone curves can be divided into three loading stages, including elastic stage, hardening stage and degradation stage. It is worth mentioning that the backbone curve can remain linear before reaching the elastic limit point.

(2) The crack load of CFST-1 is 66.17% higher than that of SRC-1 with the identical ACR, Furthermore, the yield load, peak load and ultimate load of CFST-1 are 97.84%, 82.5% and 100.3% higher than those of SPC-1, respectively. It can be concluded that the steel layout is one of the critical factors that has a significant effect on the seismic mechanical performance of transition steel-concrete composite structures.

(3) The degradation curves are relatively steep for higher ACR, it can be attributed to *P-Delta* geometric nonlinearity effects. The strength degeneration for SRC-RC transition connections is more severe than that of CFST-RC connections. On the contrary, the specimens with lower ACR can sustain higher strength at the ultimate point.

(4) Due to the triaxial compression of the CFST inner core concrete, the concrete in the steel tube can sustain higher loads while the unconfined concrete of the SRC series specimen was more prone to failure under the similar loading. After the higher vertical load applying to the top column, the confined effect of inner concrete in CFST columns is enhanced, thus the higher ACR has beneficial effect on the maximum bearing capacity, it is similar to the confined concrete in the SRC series specimen. However, due to no constraint for the unconfined concrete in SRC connections, the higher ACR reduces the lateral strength capacity for the SRC-RC transition connections. It is the most important reason of lower displacement ductility for SRC-RC transition specimens.

3.4 Energy dissipation capacity

The energy dissipation of a structural component reflects its seismic energy absorption ability (Constantinou and Symans 1992), and is usually measured by the area surrounded by the hysteresis curves. To quantify this indicator, the equivalent viscous damping coefficient h_e is

Table 2 Characteristic values

Specimen	Loading direction	Crack point		Yield point		Peak point		Ultimate point		Ductility
		F_{cr} /kN	Δ_{cr} /mm	F_y /kN	Δ_y /mm	F_m /kN	Δ_m /mm	F_u /kN	Δ_u /mm	
CFST-1	Positive	19.89	8.01	52.25	32.31	67.31	83.67	57.21	150.59	4.42
	Negative	-20.17	-4.9	-58.2	-34.77	-76.41	-83.97	-64.95	-145.08	
CFST-2	Positive	30.06	8.1	45.08	20.18	66.45	59.98	56.49	121.35	5.54
	Negative	-30.59	-8.38	-60.29	-24.12	-85.11	-60	-72.34	-122.33	
SRC-1	Positive	11.97	6.91	26.41	22.36	33.6	47.96	28.56	84.16	3.50
	Negative	-12.15	-5.6	-23.54	-24.23	-32.29	-63.02	-27.44	-90.61	
SRC-2	Positive	15.89	8.88	20.55	18.23	26.5	37.99	22.53	57.94	3.31
	Negative	-15.88	-5.45	-22.12	-14.08	-33.4	-42.01	-28.39	-49.0	

Table 3 Equivalent viscous damping coefficients

Specimen	h_{ey}	h_{em}	h_{eu}
CFST-1	0.093	0.183	0.281
CFST-2	0.115	0.177	0.306
SRC-1	0.115	0.161	0.289
SRC-2	0.169	0.221	0.338

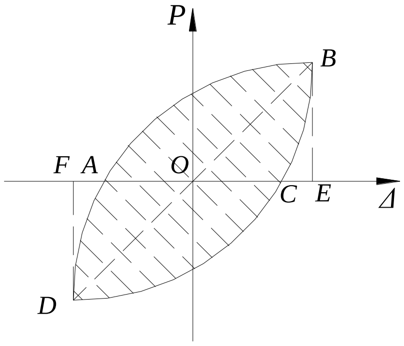

Fig. 11 Calculation of energy dissipation capacity

calculated using Eq. (1) to assess the accurate energy dissipation ability. The values of the equivalent viscous damping coefficient h_e at characteristic points are listed in Table 3. The equivalent viscous damping coefficients include h_{ey}, h_{em}, h_{eu} corresponding to the yield point, peak point and ultimate point, respectively.

$$h_e = S_{(ABC+CDA)} / (2\pi \cdot S_{(OBE+ODF)}) \quad (1)$$

where $S_{(ABD+CDA)}$ is the shadow area and $S_{(OBE+ODF)}$ is calculated by the sum area of triangles OBE and ODF in Fig. 11.

In general, the dissipated energy increases as the loading proceeds. The average values of equivalent viscous damping coefficients of the four specimens are 0.123, 0.186 and 0.304 corresponding to the yielding point, peak point and ultimate point, respectively, which shows that the transition steel-concrete composite connections have great energy dissipating capacity.

Fig. 12 illustrates the influence of axial compression ratio and steel form on energy dissipation of transition composite connections. The following observations can be addressed from Table 3 and Fig. 12.

(1) For CFST-RC transitions, the axial compression ratio doesn't play an important role in the damping behavior. CFST-1 and CFST-2 dissipate almost the same amount of energy at the different loading stage. However, for SRC-RC connections, when compared with SRC-1, whose ACR is 0.3, the h_{ey}, h_{em} and h_{eu} of SRC-2 is 47%, 37% and 17% higher, respectively. The influence of ACR on the energy dissipation of damaged SRC-RC connections is not as obvious as the original connections.

(2) When compared SRC-1 and CFST-1 with ACR of 0.3, not too much difference of equivalent viscous damping coefficient is observed. Bur for larger ACR of 0.6, the I-shaped steel connection dissipated more energy than the CFST connections at each loading stage. Thus, the steel form should be considered seriously in the actual high ACR engineering applications.

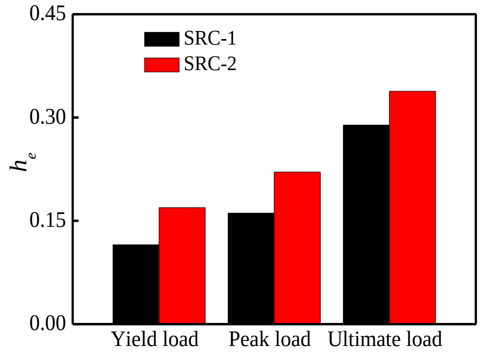

(a) The influence of axial compression ratio

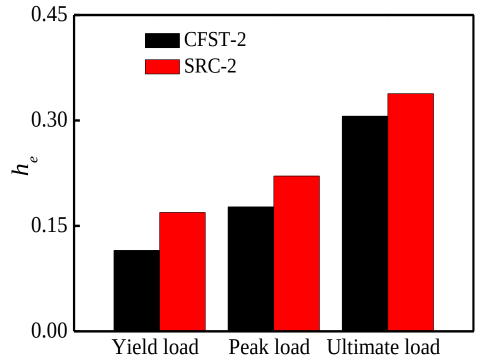

(b) The influence of steel form

Fig. 12 The influence of different design parameters on equivalent viscous damping coefficients

(3) The effect of different ACR on CFST-RC and SRC-RC can be reflected from the damage phenomenon, the cracks developed faster on SRC-2, and the spalling and crush of the concrete cover was much more serious on SRC-2 than that on SRC-1, which dissipates more energy during loading. However, similar damage was only observed at the bottom of lower RC parts for both of CFST-1 and CFST-2, the upper peripheral steel tube protected the inner concrete from crushing. This didn't change the dissipated energy considerably.

3.5 Stiffness degradation

With the increasing load, the damage propagates and the structural secant stiffness decreases gradually. The stiffness degradation tendency can be obtained to describe the cumulative damage effect. The secant stiffness was calculated at the first cycle of each loading level. Fig. 13 shows the relationship between the ratio of secant stiffness (K_i) to yield stiffness and the ratio of lateral displacements to the absolute value of yield displacement ($\Delta/|\Delta_y|$).

It can be seen from Fig. 13 that the trends of stiffness degradation for the four specimens are similar. The stiffness deteriorates rapidly in the initial loading stages while the curves tend to be stable after the specimens completely enter the plastic stage. It can also be concluded that the secant stiffness decreases faster for CFST-RC transition connections with lower ACR than the one with greater ARC, while no such tendency is observed for SRC-RC transition connections.

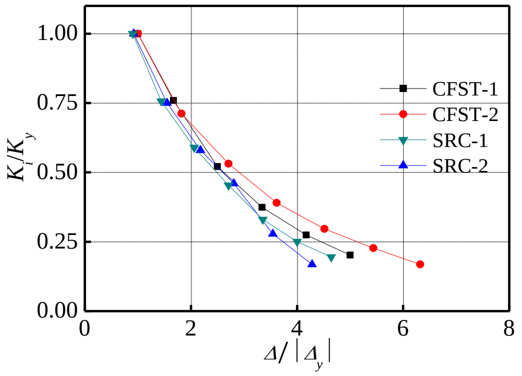

Fig. 13 Stiffness degradation

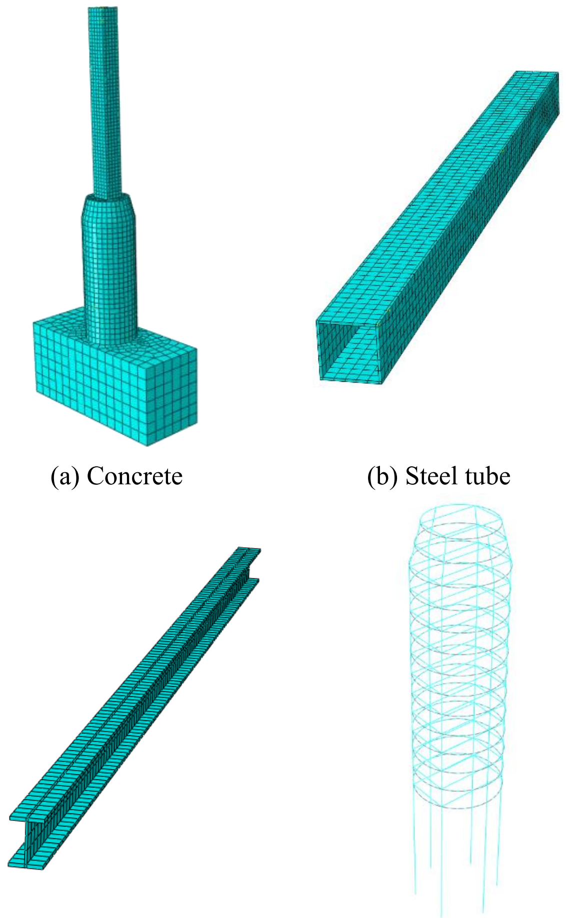

(a) Concrete (b) Steel tube

(c) I-shaped steel (d) Steel bars

Fig. 14 FE models

4. Nonlinear static pushover analysis

4.1 FE model construction

Based on the above experiments, the FE model was established in ABAQUS, with an approximate mesh size of 30 mm for the specimens and 100 mm for the ground beam, to investigate more detailed mechanical behavior about the seismic performance of CFST-RC transition connection and SRC-RC transition connection subassemblies. Eight-node solid reduced elements (C3D8R) were utilized for the concrete and steel, except two-node 3D truss elements for steel bars. The three-dimensional model is shown in Fig. 14.

The material constitutive model is very crucial in predicting the real structural behavior. To better track the material properties, the concrete damaged plasticity model was employed.

For confined concrete, including CFST inner concrete and SRC confined concrete, the restraint effect (Han *et al.* 2001) was taken into consideration. According to the confined concrete theory and method, the restraint index ξ, calculated by Eq. (2), was deployed to simulate the composite action between the concrete and steel.

$$\xi=\frac{A_s f_y}{A_c f_{ck}} \tag{2}$$

where A_s and A_c denote the sectional area of steel and concrete, f_y and f_{ck} represent the yield strength of steel and the standard value of axial compression strength of concrete, respectively.

Based on the stress-strain constitute model of the confined concrete (Liu 2005), the following equations were used in this model.

$$y=\begin{cases} 2\cdot x-x^2 & (x\le 1) \\ \dfrac{x}{\beta_0\cdot(x-1)^{\eta}+x} & (x\ge 1) \end{cases} \tag{3}$$

where $x=\dfrac{\varepsilon}{\varepsilon_0}$, $y=\dfrac{\sigma}{\sigma_0}$, σ_0 and ε_0 are the axial compressive strength of concrete and corresponding compressive strain, respectively. For square sections, the correction factor $\eta=1.6+1.5/x$, $\beta_0=\dfrac{\sigma_0^{0.1}}{1.2\sqrt{1+\xi}}$.

The compression and tension behaviors of unconfined concrete are in accordance to the Chinese Concrete Design Code (GB 50010-2010). The dilation angle, eccentricity, the ratio of biaxial to uniaxial strength and ratio of normal stress between tension meridian and compression meridian are set at 30, 0.1, 1.16 and 2/3, respectively (Chen 2013).

The damage factor d_c describes the cumulative damage of concrete, and it reflects the material degradation properties. The following equations can be adopted to calculate the damage factor.

$$d_c=\begin{cases} 1-\dfrac{\rho_c n}{n-1+x^n} & (x=\varepsilon/\varepsilon_0\le 1) \\ 1-\dfrac{\rho_c}{\alpha_c(x-1)^2+x} & (x=\varepsilon/\varepsilon_0>1) \end{cases} \tag{4}$$

$$\rho_c=\frac{\sigma_0}{E_c+\varepsilon_0} \tag{5}$$

$$n=\frac{E_c\varepsilon_0}{E_c\varepsilon_0-\sigma_0} \tag{6}$$

The ideal elastic-plastic hardening model was used to simulate the steel behavior. The hardening ratio is set at 0.01 after steel yielding. The other mechanical properties were obtained from the material coupon test.

In the actual quasi-test, the steel studs were deployed to mitigate the relative slip between the steel and concrete,

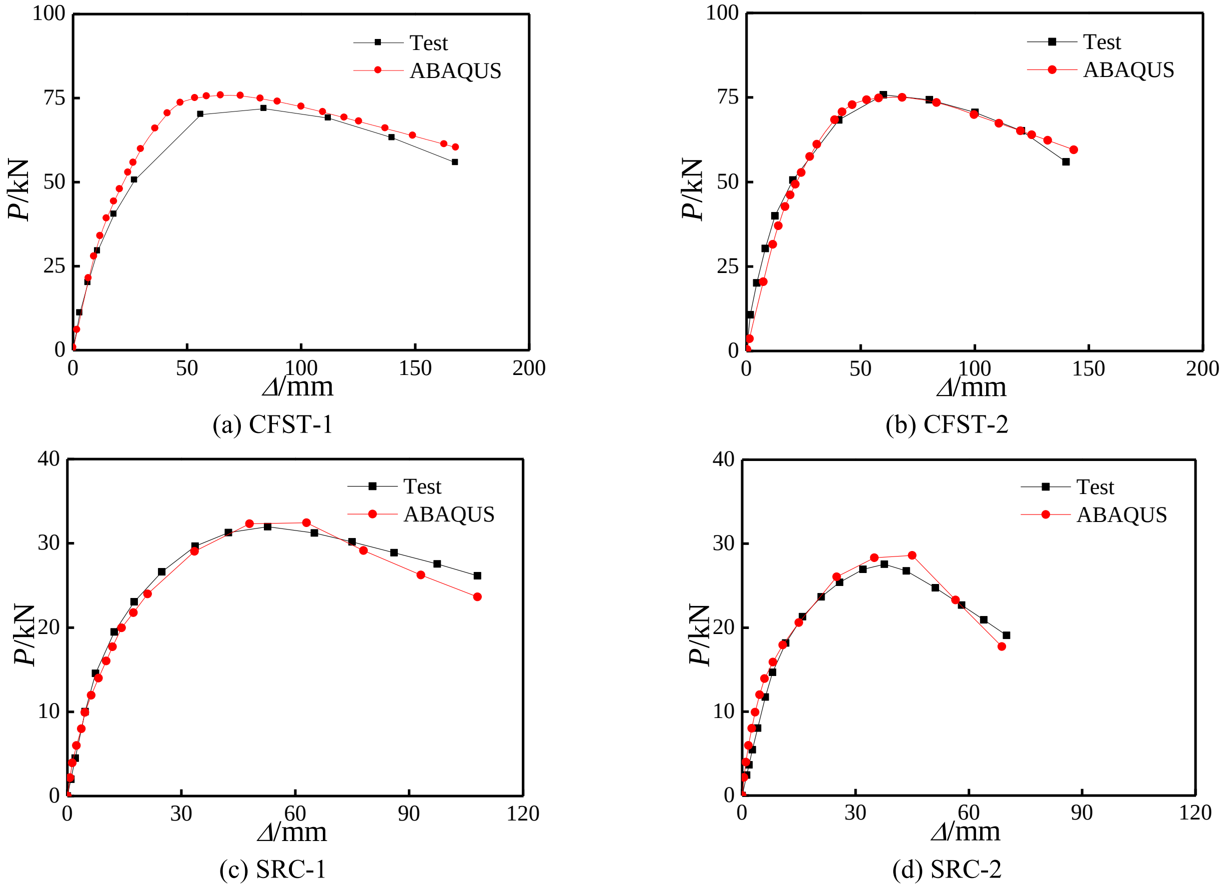

Fig. 15 Comparison of backbone curves

Table 4 Comparison between FEM and test

Specimen		Yield point		Peak point		Ultimate point	
		P_y/kN	Δ_y/mm	P_m/kN	Δ_m/mm	P_u/kN	Δ_u/mm
CFST-1	Test	55.23	33.54	71.86	83.82	61.08	147.84
	ABAQUS	59.83	30.01	76.45	68.38	64.45	145.32
	Error/%	8.33	10.52	6.39	18.42	5.52	1.70
CFST-2	Test	52.69	22.15	75.78	59.99	64.42	121.84
	ABAQUS	58.08	28.18	75.05	63.03	63.79	123.33
	Error/%	10.23	27.22	0.96	5.07	0.98	1.22
SRC-3	Test	24.97	23.30	32.94	55.49	28.00	87.39
	ABAQUS	25.25	21.85	31.97	52.78	27.18	100.37
	Error/%	1.13	6.62	2.95	4.87	3.04	14.85
SRC-4	Test	21.33	16.15	29.95	40.00	25.46	53.47
	ABAQUS	22.31	18.63	27.54	37.66	23.41	55.65
	Error/%	4.59	15.35	8.04	5.86	8.04	4.09

thus the ideal embedding interaction was defined in the model to describe the relation between steel, steel bar and concrete, no slip effect was taken into consideration. On the other hand, the influence of residual stress was not as obvious as bare steel components because the steel was surrounded by concrete, thus the original residual stress of steel was not inputted. To simplify the model and save the computation time, it should be pointed out that the FEM studies described herein did not address the issue of fracture propagation.

4.2 Validation of FE models

The backbone curves from the finite element analyses were compared with the experimental results, as shown in Fig. 15 and Table 4.

The calculated initial stiffness agrees well with the experiments for the specimens with smaller ACR (CFST-1 and SRC-1), while acceptable differences appear when compare to specimens with larger ACR (CFST-2 and SRC-2). The reason is the confined concrete is in more severe compressive stress when applying higher axial compression force, the constraint effect is more obvious but the confined concrete in the model is simplified by restraint index ξ, which is, to certain extent, misaligned to the actual situations. Additionally, the small out-of-plane deformation in the actual experiment may also result in this mismatch and this influence is slightly more obvious for specimens with ACR of 0.6 than that with 0.3 because of the *P*-Δ effect. Besides that, the bond-slip effect between two materials, which is not considered in the model, can lead to the earlier strength degradation and failure of the experiment.

4.3 Further parametric investigations

Due to the irregular and complex layout of transition steel-concrete composite structures, there is high demand for further study of various mechanical parameters. In this study, the concrete strength, steel grade and longitudinal

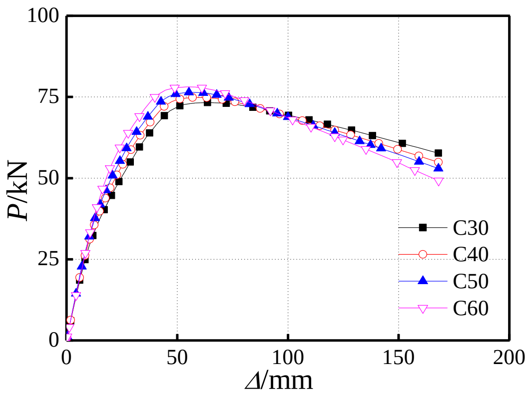

(a) CFST-RC transition connections

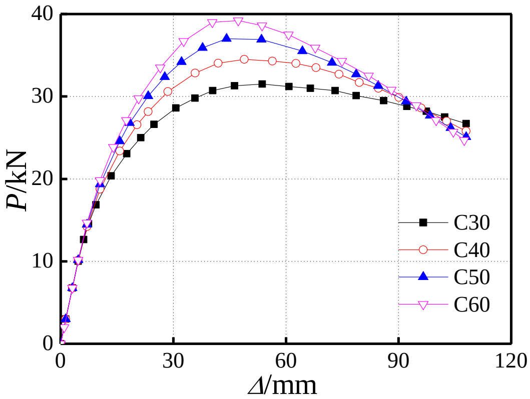

(b) SRC-RC transition connections

Fig. 16 The influence of concrete strength

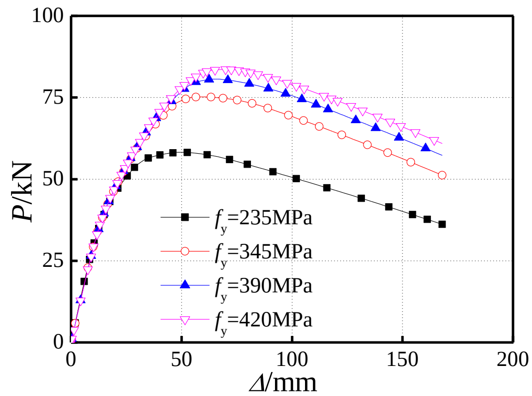

(a) CFST-RC transition connections

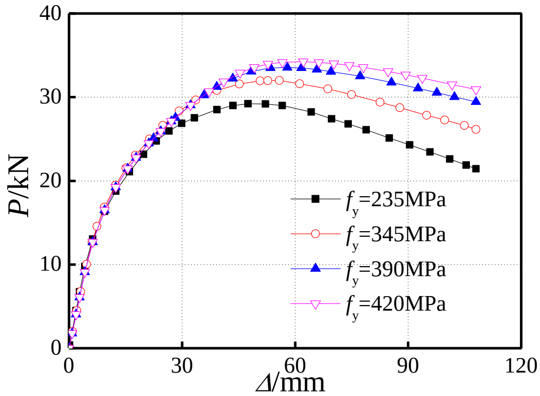

(b) SRC-RC transition connections

Fig. 17 The influence of steel grade

reinforcement ratio of RC columns are further investigated.

4.3.1 Concrete strength (f_{cu})

As mentioned above, the damage pattern for CFST-RC transition connections was circular crack around the RC column. For SRC-RC transition connections, obvious failure and plastic hinges of concrete were observed at the upper SRC column base. Four concrete strength were studied to evaluate its effect on the seismic performance of transition composite connections, including C30, C40, C50 and C60 (the values correspond to cubic compressive standard strength). The influence of concrete strength is shown in Fig. 16.

The results indicate that the concrete strength has rather minimal influence on the CFST-RC transition connections, because most of the strength contribution is attributed to the steel tube at the upper columns. However, the most crucial part of the SRC-RC transition connections is the unconfined concrete at the upper column, compared with C30 concrete, the peak strength of C40, C50 and C60 increased about 9.42%, 17.69% and 25.49%, respectively. It can be concluded that the influence of concrete strength is more significant for SRC-RC transition connections than that of CFST-RC transition connections. For the two different steel layout transition connections, the similarity is that the higher the concrete strength, the quicker and more obvious decreasing trend of the backbone curves after the peak point, the brittle behavior of high strength concrete is responsible to this kind of phenomenon.

4.3.2 Steel grade (fy)

The influence of steel grades on the transition steel-concrete composite structures was investigated by adopting four different steel grades. As mentioned above, the concrete cracks first occurred, followed by the yielding of the steel tube for CFST-RC series connections, and most of the strength contribution is coming from the steel tube. From Fig. 17, it can be concluded that steel grade plays the most important role in increasing the bearing capacity of CFST-RC connections. The load-carrying capacities of the specimens with steel yield strengths of 345 MPa, 390 MPa and 420 MPa are increased by 29.16%, 38.46% and 43.58% respectively when compared with f_y=235 MPa model. For SRC-RC connections, the steel plate takes the predominant role after the unconfined concrete loses its load carrying capacity. The post-peak response becomes mild for larger steel yield strength specimen. Moreover, the displacement ductility for Q235, and Q345 are not significantly different while the ductility reduces obviously for Q390 and Q420. Thus, an appropriate steel grade is of great importance for the structural ductile design.

4.3.3 Longitudinal reinforcement ratio (ρ) of RC columns

To further study the contribution of lower circular RC columns to the entire transition connections, the longitudinal reinforcement ratio was investigated herein.

Fig. 18 shows the influence of longitudinal reinforcement ratio to the two series transition connections.

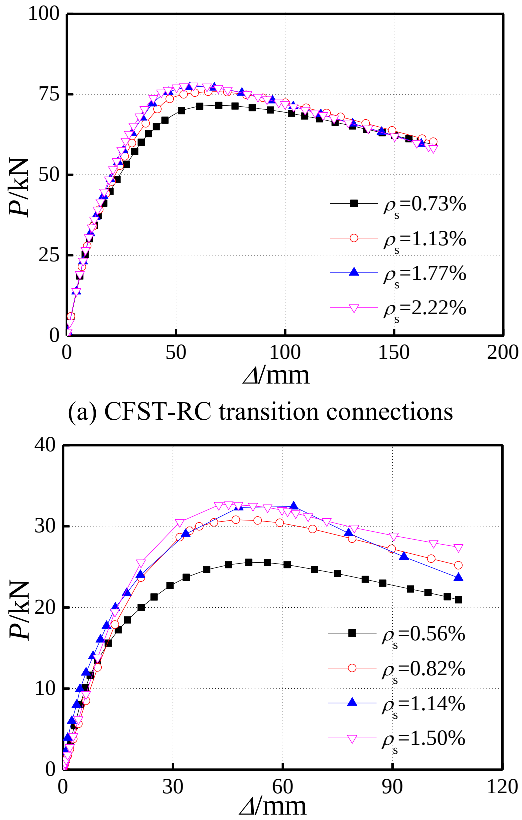

(b) SRC-RC transition connections

Fig. 18 The influence of longitudinal reinforcement ratio of RC columns

Except for the ρ=0.56% SRC-RC specimen, the longitudinal reinforcement ratio does not markedly change the backbone curves. The initial stiffness is almost the same for the most cases, this indicates that the reinforcement ratio is not as significantly important as the steel plate grade in transition composite connections. For SRC-RC specimen with ρ=0.56%, the load-bearing capacity decreases about 20.6% when compared to SRC-RC model with ρ=1.50%. The most obvious reason for this phenomenon is the different failure mode for this configuration, the plastic hinges generate at the lower RC column base and the vertical longitudinal bar yield before the damage of upper SRC column for ρ=0.56% SRC-RC specimen, no yielding is observed in the I-shaped steel and longitudinal bar in the upper columns. Thus, the longitudinal reinforcement ratio and steel ratio should be balanced in the actual SRC-RC engineering applications

5. Conclusions

Based on the lateral reversed cyclic loading test and numerical analyses of four transition steel-composite composite connections with different steel layout forms, the following conclusions can be highlighted:

1. Different steel layouts produced significantly different failure modes. For CFST-RC transition specimens, the circular cracks of concrete at the RC column base was followed by steel yielding at the bottom of the CFST column. While uncoordinated deformation could be observed between SRC and RC columns in SRC-RC transition specimens, the crushing and peeling damage of unconfined concrete at the SRC column base was more serious.
2. The influence of axial compression ratio on the hysteretic behavior is evident, the compatible deformation capacity of the smaller ACR specimen is slightly better. When ACR increases, the hysteresis curve becomes fuller, while the displacement ductility reduced and the stiffness degradation rate is faster. Moreover, the existence of steel tube and I-shape steel makes the transition steel-concrete composite connections behave similarly to bare steel members.
3. Due to the triaxial compression of the CFST inner core concrete, the concrete in the steel tube can sustain higher loads while the unconfined concrete of the SRC-RC series specimen experienced significant damage. After the higher vertical load applying to the top column, the confined effect of inner concrete in CFST columns is enhanced, thus the higher ACR plays a positive role in the load bearing capacity. However, higher ACR means the unconfined concrete cover needs to sustain larger negative compressive strength, which in turn decreases the lateral strength capacity for the entire SRC-RC transition connections.
4. Based on the experimental configurations, a high-fidelity ABAQUS model was established to further study the mechanical behavior of transition composite connections. The results indicate that concrete strength has a moderate effect on the CFST-RC transition connections but the more significant influence on SRC-RC connections. The steel grade plays the most important role in increasing the bearing capacity of transition steel-concrete composite connections, and the strength decreasing trend after peak value becomes mild for the specimens with higher steel yield strength. A balance needs to be found between the longitudinal reinforcement ratio and steel ratio in the actual SRC-RC engineering applications.

Acknowledgements

The authors would like to thank the support provided by the National Natural Science Foundation of China (Grant No. 51678478) and National Science and Technology Support Program of the 12th Five-Year (Grant No. 2014BAL06B03).

References

GB 50010 (2010), Code for Design of Concrete Structures, China Architecture & Building Press, Beijing.

GB/T 2975 (1998), Steel and Steel Products-location and Preparation of Test Pieces for Mechanical Testing, State Bureau of Quality Technical Supervision, Beijing.

JGJ 138 (2001), Technical Specification for Steel Reinforced Concrete Composite Structures, China Architecture & Building

Press, Beijing.
JGJ 138 (2016), Code for Design of Composite Structures, China Architecture & Building Press, Beijing.
Chen, M. (2013), "Research on the mechanical behavior and abaqus analysis of joints between steel beams and concrete filled rectangular steel tube column", Xi'an University of Architecture and Technology, Xi'an.
Chen, Z., Xu, J., Chen, Y. and Xue, J. (2015), "Seismic behavior of steel reinforced concrete (SRC) T-shaped column-beam planar and 3D hybrid joints under cyclic loads", *Earthq. Struct.*, **8**(3), 555-572.
Constantinou, M.C. and Symans, M. (1992), "Experimental and analytical investigation of seismic response of structures with supplemental fluid viscous dampers", National Center for Earthquake Engineering Research Buffalo, NY.
D'Ambrisi, A. and Filippou, F.C. (1999), "Modeling of cyclic shear behavior in RC members", *J. Struct. Eng.*, **125**(10), 1143-1150.
Fu, Y.Y., Yan, S.W. and Du, C. (2011), "Performance analysis of CFST column and RC Column subjected to eccentric load", *Appl. Mech. Mater*., **94**, 805-809.
Han, L. and An, Y. (2014), "Performance of concrete-encased CFST stub columns under axial compression", *J. Constr. Steel Res*., **93** 62-76.
Han, L., Tao, Z. and Liu, W. (2001), "Concrete filled steel tubular structures from theory to practice", *J. Fuzhou Univ. (Nat. Sci. Ed.)*, **6**, 24-34.
Kunnath, S.K., Mander, J.B. and Fang, L. (1997), "Parameter identification for degrading and pinched hysteretic structural concrete systems", *Eng. Struct*., **19**(3), 224-232.
Liu, W. (2005), "Research on mechanism of concrete-filled steel tubes subjected to local compression", Fuzhou University, Fuzhou.
Lowes, L.N. and Altoontash, A. (2003), "Modeling reinforced-concrete beam-column joints subjected to cyclic loading", *J. Struct. Eng.*, **129**(12), 1686-1697.
Qi, L. and Xue, J. (2018), "Pseudo dynamic test and time-history analyses of traditional-style steel frame structures", *Int. J. Steel Struct*., **18**, 402-416.
Qi, L., Xue, J. and Leon, R.T. (2017), "Experimental and analytical investigation of transition steel connections in traditional-style buildings", *Eng. Struct*., **150**, 438-450.
Qi, L., Xue, J., Zhai, L., Zhao, X. and Leon, R.T. (2018), "Experimental and numerical studies on seismic performance of traditional style steel-concrete composite frame", *Compos. Struct*., **201**, 514-527.
Tirasit, P. and Kawashima, K. (2007), "Seismic performance of square reinforced concrete columns under combined cyclic flexural and torsional loadings", *J. Earthq. Eng*., **11**(3), 425-452.
Verderame, G.M., Fabbrocino, G. and Manfredi, G. (2008), "Seismic response of RC columns with smooth reinforcement. Part II: Cyclic tests", *Eng. Struct*., **30**(9), 2289-2300.
Wang, Z., Han, L., Li, W. and Tao, Z. (2015), "Seismic performance of concrete-encased CFST piers: experimental study", *J. Bridge Eng*., **21**(4), 1-12.
Wu, K., Xue, J.Y. and Zhao, H.T. (2013), "Failure mechanism and bearing capacity of transfer columns in SRC-RC hybrid structures", *Eur. J. Environ. Civil Eng*., **17**(sup1), 205-228.
Wu, K., Xue, J., Nan, Y. and Zhao, H. (2016), "Experimental research on seismic behavior of SRC-RC transfer columns", *Steel Compos. Struct*., **21**(1), 157-175.
Wu, K., Xue, J. and Zhao, H. (2010), "Study on shear performance of SRC-RC transfer column with short column failure pattern", *Indus. Constr*., **40**(11), 51-54.
Wu, K., Xue, J., Zhao, H. and Wang, D. (2008), "Analysis of seismic performance of SRC-RC transfer column [J]", *World Earthq. Eng*., **3**, 135-139.
Xu, J., Chen, Z., Zhao, X., Demartino, C., Ozbakkaloglu, T. and Xue, J. (2019), "Seismic performance of circular recycled aggregate concrete-filled steel tubular columns: FEM modelling and sensitivity analysis", *Thin Wall. Struct*., **141**, 509-525.
Xue, J. and Qi, L. (2016), "Experimental studies on steel frame structures of traditional-style buildings", *Steel Compos. Struct*., **22**(2), 235-255.
Xue, J., Qi, L., Gao, L. and Liu, Z. (2016), "Mechanical behavior of lattice steel reinforced concrete inner frame with irregular section columns under cyclic reversed loading", *Eng. Struct*., **128**, 225-236.
Yadav, R., Yuan, H., Chen, B. and Lian, Z. (2018), "Experimental study on seismic performance of latticed CFST-RC column connected with RC web", *Thin Wall. Struct*., **126**, 258-265.

CC

Nomenclature

K	Coefficient for effective length
L	Geometric length
r	Radius of gyration
ρ	Reinforcement ratio
f_y	Yield strength of steel
ε_y	Yield strain of steel
f_u	Ultimate strength of steel
f_{ck}	Standard value of axial compression strength
E_s	Elastic modulus of steel
E_c	Elastic modulus of concrete
f_{cu}	Cubic compressive strength of concrete
P	Horizontal force
F_{cr}, Δ_{cr}	Crack load and corresponding displacement
F_y, Δ_y	Yield load and corresponding displacement
F_m, Δ_m	Peak load and corresponding displacement
F_u, Δ_u	Ultimate load and corresponding displacement
h_{ey}, h_{em}, h_{eu}	Equivalent viscous damping coefficient corresponding to the yield load, peak load and ultimate load, respectively
K_i	Secant stiffness
ξ	Restraint index
A_s	Sectional area of steel
A_c	Sectional area of concrete
σ_0, ε_0	Axial compressive strength of concrete and the corresponding strain